nature COMMUNICATIONS

ARTICLE

Received 21 Sep 2014 | Accepted 28 Nov 2014 | Published 14 Jan 2015

DOI: 10.1038/ncomms6982 OPEN

An efficient molybdenum disulfide/cobalt diselenide hybrid catalyst for electrochemical hydrogen generation

Min-Rui Gao[1,*], Jin-Xia Liang[2,3,*], Ya-Rong Zheng[1], Yun-Fei Xu[1], Jun Jiang[1], Qiang Gao[1], Jun Li[2] & Shu-Hong Yu[1]

The electroreduction of water for sustainable hydrogen production is a critical component of several developing clean-energy technologies, such as water splitting and fuel cells. However, finding a cheap and efficient alternative catalyst to replace currently used platinum-based catalysts is still a prerequisite for the commercialization of these technologies. Here we report a robust and highly active catalyst for hydrogen evolution reaction that is constructed by *in situ* growth of molybdenum disulfide on the surface of cobalt diselenide. In acidic media, the molybdenum disulfide/cobalt diselenide catalyst exhibits fast hydrogen evolution kinetics with onset potential of −11 mV and Tafel slope of 36 mV per decade, which is the best among the non-noble metal hydrogen evolution catalysts and even approaches to the commercial platinum/carbon catalyst. The high hydrogen evolution activity of molybdenum disulfide/cobalt diselenide hybrid is likely due to the electrocatalytic synergistic effects between hydrogen evolution-active molybdenum disulfide and cobalt diselenide materials and the much increased catalytic sites.

[1] Division of Nanomaterials & Chemistry, Hefei National Laboratory for Physical Sciences at Microscale, Collaborative Innovation Center of Suzhou Nano Science and Technology, Department of Chemistry, University of Science and Technology of China, Hefei 230026, China. [2] Key Laboratory of Organic Optoelectronics and Molecular Engineering of Ministry of Education, Department of Chemistry, Tsinghua University, Beijing 100084, China. [3] Guizhou Provincial Key Laboratory of Computational Nano-Material Science, Guizhou Normal College, Guiyang 550018, China. * These authors contributed equally to this work. Correspondence and requests for materials should be addressed to S.-H.Y. (email: shyu@ustc.edu.cn).

Owing to their diffuse nature, electricity from renewable but intermittent energy (for example, solar and wind) must be stored durably for off-grid applications. Electrochemical water splitting to produce hydrogen (H_2) offers a promising and sustainable solution for this purpose by converting such electricity energy into stable chemical bonds[1,2]. Appropriate electrocatalysts, such as platinum (Pt) and its alloys, play a vital role in the H_2 evolution reaction (HER) because they can catalyse the conversion from a pair of protons and electrons to H_2 at high reaction rates and low overpotentials (η)[1–3]. However, the prohibitive cost and scarcity of Pt pose tremendous limitations to widespread use. Therefore, finding robust and efficient alternative catalysts that are geologically abundant is crucial to the future of 'hydrogen economy'.

Molybdenum disulfide (MoS_2), a widely used industrial catalyst for hydrodesulfurization[4], has recently demonstrated promise as effective HER catalyst based on both computational and experimental studies[5,6]. The HER activity was discovered to arise from the exposed (10–10) planes on edges of MoS_2, whereas the (0001) basal planes are catalytically inactive[5–7]. This understanding has led to great efforts to develop highly nanostructured MoS_2-based HER catalysts to maximize the number of edge sites, including crystalline[8–12] and amorphous materials[13–15], MoS_2-based hybrid materials[16–19] and molecular mimics[7]. Despite significant success, the design and fabrication of MoS_2-based HER electrocatalysts with satisfactory activity and stability remain a big challenge.

In recent years, we have been making efforts to explore efficient electrocatalysts by using Earth-abundant 3*d* metal (Co, Ni and so on) chalcogenides[20–27]. New NiSe nanofibres[24] and lamellar mesostructured $CoSe_2$/DETA (DETA, diethylenetriamine) nanobelts[25] were found to show decent HER activity in acidic electrolyte. Kong *et al.*[28] also observed good HER activities from various polycrystalline transition metal dichalcogenide (ME_2, M = Fe, Co, Ni; E = S, Se) films, especially from the $CoSe_2$. Recently, we found that the HER activity of $CoSe_2$ nanobelts can be improved greatly after anchoring Ni/NiO nanoparticles onto their surfaces[25]. The synergetic chemical coupling effects between $CoSe_2$ and grafted Ni/NiO were believed to contribute to the enhancement. Similar promoted performances have also been observed on MoS_2/graphene[16,17], MoO_3/MoS_2 (ref. 18) and MoS_2/Au (ref. 19) composite catalysts for H_2 production. These works point to the possibility to access new and efficient HER catalysts by combining the promising $CoSe_2$ and MoS_2.

We report here that a HER electrocatalyst based on quasi-amorphous MoS_2-coated $CoSe_2$ (denoted as $MoS_2/CoSe_2$) hybrid is highly active and stable in acidic electrolyte. Notably, without any noble metals, the $MoS_2/CoSe_2$ hybrid catalyst shows an onset potential close to commercial Pt catalyst (Johnson-Matthey, 20 wt% Pt/XC-72) and a small Tafel slope of ~36 mV per decade as well as no current loss after long-term chronoamperometry measurement, performing the best among the noble-metal-free HER electrocatalysts. These results suggest a strategy for designing non-noble metal catalysts with enhanced HER performance that is comparable to the state-of-the-art Pt-based catalysts.

Results

$MoS_2/CoSe_2$ hybrid catalyst. The $MoS_2/CoSe_2$ hybrid was prepared directly in a closed *N*,*N*-dimethylformamide (DMF)/hydrazine solvothermal system, where $(NH_4)_2MoS_4$ was used as a precursor for growing MoS_2 around the freshly made $CoSe_2$/DETA nanobelt substrates (Fig. 1a; Supplementary Fig. 1; see Methods for details of the synthesis). The MoS_2-coated $CoSe_2$ hybrid was shown by means of scanning electron microscopy and transmission electron microscopy (TEM; Fig. 2a–c), which revealed the compact graphene-like MoS_2 nanosheets grown on the surface of $CoSe_2$ with a partially free-standing branch-like feature (Supplementary Fig. 2). Substantial amino groups on the $CoSe_2$/DETA surface (Supplementary Fig. 3) serve as nucleation sites for coupling Mo precursor and subsequently reduced to MoS_2 on $CoSe_2$ (refs 21,23). A control experiment performed under identical synthesis conditions, but without $CoSe_2$ nanobelts, produced three-dimensional (3D) aggregates of MoS_2 sheets (Fig. 1b; Supplementary Fig. 4), suggesting that $CoSe_2$ could be a useful support for mediating the growth of loaded materials and constructing novel functional hybrids.

Figure 2d presents high-resolution TEM (HRTEM) images of the $MoS_2/CoSe_2$ hybrid. Layered MoS_2 (often less than five layers) nanosheets, with an interlayer separation of 0.63 nm, were grown intimately on the $CoSe_2$ substrate. High-crystalline $CoSe_2$ substrate with *d* spacing of 0.27 nm can be seen frequently through the interspace of grafted MoS_2 (see Supplementary Fig. 5 for additional images). This non-fully covered structure may take advantage of merits from both MoS_2 and $CoSe_2$ for catalysing H_2 evolution. Selected area electron diffraction (SAED) pattern (inset in Fig. 2c; Supplementary Fig. 6) revealed clear diffraction spots (marked by yellow arrows) from single-crystalline $CoSe_2$ support (JCPDS 9-0234) and also faint diffraction rings from grafted MoS_2 (JCPDS 77-1716). These barely recognizable diffraction rings indicate the quasi-amorphous structure of MoS_2, consistent with the X-ray diffraction (XRD) data of $MoS_2/CoSe_2$ with broadening diffraction peaks (Fig. 2e). Inasmuch as amorphous MoS_2 has recently been demonstrated to be effective HER catalysts[13–15] for its abundant defects and resultant more active edge sites[29], we thus infer that the quasi-amorphous MoS_2 modification may benefit the hybrid material to catalytically evolve H_2. Energy-dispersive X-ray spectrum (EDX; Fig. 2f) analysis further confirmed the formation of $MoS_2/CoSe_2$ hybrid with Co, Se, Mo and S as the principal elemental components (Cu and C peaks emanate from the carbon-coated TEM grid), agreeing with the X-ray photoelectron spectroscopy (XPS) results (Supplementary Fig. 7). Scanning TEM (STEM) and EDX elemental mappings revealed uniform spatial distribution of Co, Se, Mo and S over the marked detection range of the constructed hybrid material (Fig. 2g).

Catalytic hydrogen evolution. To assess the HER electrocatalytic activity, thin film of various catalysts was prepared on glassy carbon (GC) electrodes for cyclic voltammetry in H_2-saturated 0.5 M H_2SO_4 electrolyte (see Methods for experimental details). Potentials were measured vs saturated calomel electrode (SCE) and are reported vs reversible hydrogen electrode (RHE). The electrode was kept rotating (1,600 r.p.m.) during the measurements to remove *in situ*-emerged H_2 bubbles. Figure 3a shows that GC electrode guarantees a minimal background activity for H_2 evolution. A reductive sweep of $MoS_2/CoSe_2$ hybrid showed a low η of 11 mV for the HER, beyond which a sharp increase in cathodic current was observed, corresponding to catalytic H_2 evolution (Fig. 3a; Supplementary Fig. 9). By contrast, pure $CoSe_2$ nanobelts exhibited inferior HER activity with a larger onset potential of ~50 mV and lower catalytic current, while pure MoS_2 nanosheet aggregates only affected little HER activity. The HER kinetics of the above catalysts was probed by corresponding Tafel plots ($\log j \sim \eta$) (Fig. 3b). Tafel slope of ~36 mV per decade was measured for $MoS_2/CoSe_2$ hybrid, which is close to the value of 30 mV per decade for Pt/C catalyst and lower than that of 48 mV per decade for $CoSe_2$ and 101 mV per decade for 3D MoS_2 aggregates (Table 1). This Tafel slope is also comparable to or

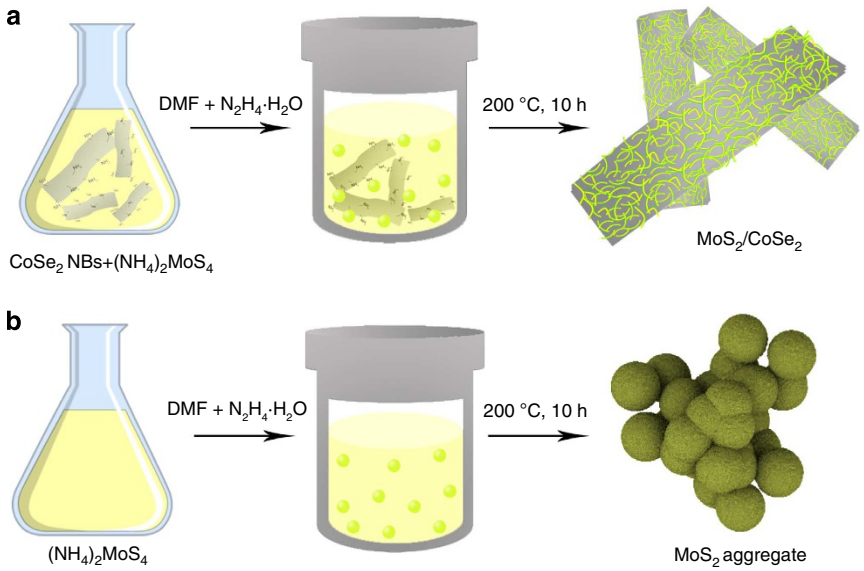

Figure 1 | Schematic illustration of the preparation of $MoS_2/CoSe_2$ hybrid. (**a**) Solvothermal synthesis with $CoSe_2$/DETA nanobelts as substrates for preparation of $MoS_2/CoSe_2$ hybrid. (**b**) Solvothermal synthesis without $CoSe_2$/DETA nanobelts leads to free MoS_2 nanosheet aggregates.

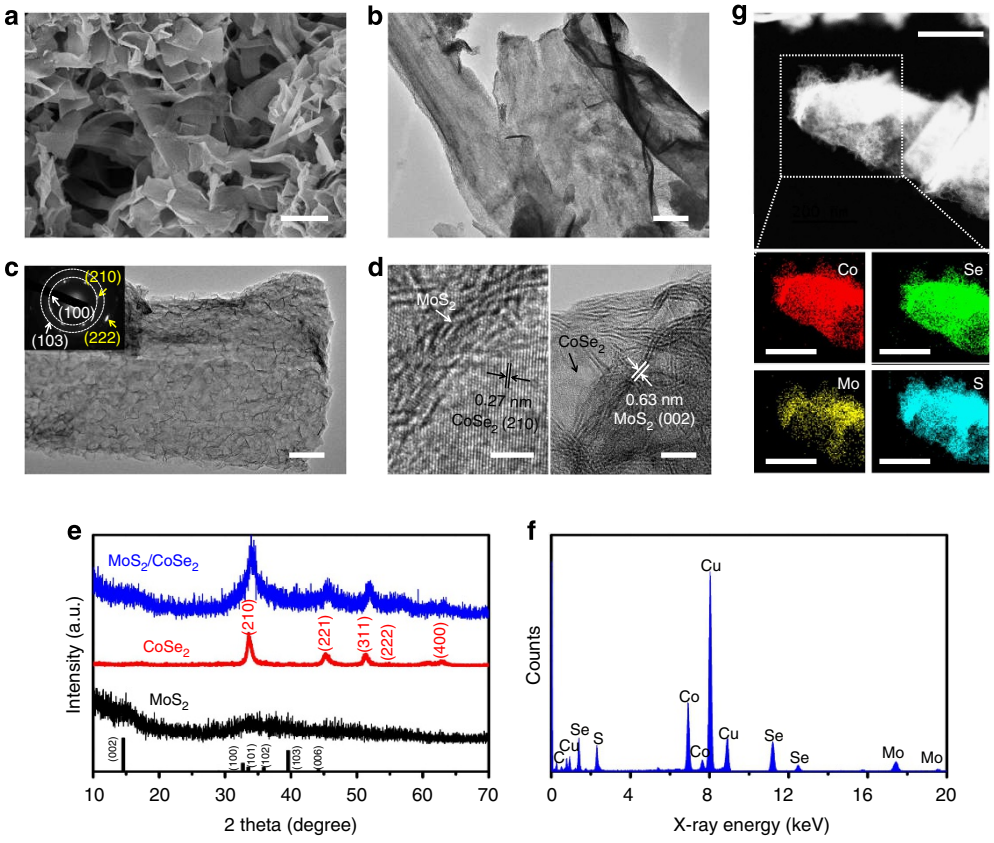

Figure 2 | Characterization of the $MoS_2/CoSe_2$ hybrid. (**a**) Scanning electron microscopy image of $MoS_2/CoSe_2$ hybrid. Scale bar, 800 nm. (**b**,**c**) TEM images with different magnifications of $MoS_2/CoSe_2$ hybrid. Scale bars, 200 and 50 nm, respectively. The inset in **c** shows corresponding SAED pattern. (**d**) HRTEM images of $MoS_2/CoSe_2$ hybrid showing distinguishable microstructures of MoS_2 and $CoSe_2$. Scale bars, 5 nm. (**e**,**f**) XRD patterns and EDX spectrum of the $MoS_2/CoSe_2$ hybrid, respectively. (**g**) STEM-EDX elemental mapping of $MoS_2/CoSe_2$ hybrid showing clearly the homogeneous distribution of Co (red), Se (green), Mo (yellow) and S (azure). Scale bars, 200 nm.

lower than that of all the reported noble-metal-free HER catalysts in the literature (Supplementary Table 1), demonstrating the superior HER kinetics of $MoS_2/CoSe_2$ hybrid. At high current densities (for example, 10 mA cm^{-2} with η of 68 mV), $MoS_2/CoSe_2$ hybrid also represents a more efficient catalyst relative to other noble-metal-free HER catalysts (Supplementary Table 1). The HER inherent activity of these catalysts was evaluated by the exchange current density (j_0). The j_0 of 7.3×10^{-2} mA cm^{-2} for $MoS_2/CoSe_2$ hybrid outperforms the values of 8.4×10^{-3} mA cm^{-2} for pure $CoSe_2$ and 9.1×10^{-4} mA cm^{-2} for pure

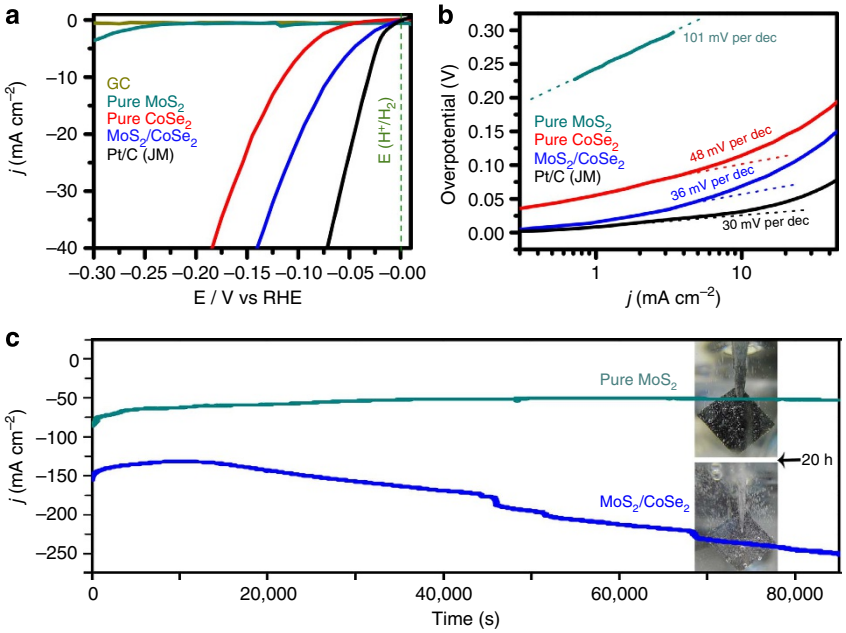

Figure 3 | Electrocatalytic hydrogen evolution of different catalysts. (**a**) Polarization curves for HER on bare GC electrode and modified GC electrodes comprising $MoS_2/CoSe_2$ hybrid, pure MoS_2, pure $CoSe_2$ and a high-quality commercial Pt/C catalyst. Catalyst loading is about 0.28 mg cm^{-2} for all samples. Sweep rate: 2 mV s^{-1}. (**b**) Tafel plot for the various catalysts derived from **a**. (**c**) Chronoamperometric responses ($j \sim t$) recorded on $MoS_2/CoSe_2$ hybrid and pure MoS_2 at a constant applied potential of -0.7 V vs SCE. The catalysts were deposited on CFP with the same loading of 1 mg cm^{-2}. Inset digital photos show the H_2 bubbles formed on MoS_2-modified CFP (up) and $MoS_2/CoSe_2$-modified CFP (down) at the time point of 20 h. All the measurements were performed in H_2-saturated 0.5 M H_2SO_4 electrolyte. dec, decade.

Table 1 | Comparison of catalytic parameters of different HER catalysts.

Catalyst	Onset potention (mV vs RHE)	Tafel slope (mV per decade)	Exchange current density (j_0, mA cm^{-2})*
MoS_2	−237	101	9.1×10^{-4}
$CoSe_2$	−50	48	8.4×10^{-3}
$MoS_2/CoSe_2$	−11	36	7.3×10^{-2}
Pt/C†	0	30	7.1×10^{-1}

HER, H_2 evolution reaction; RHE, reversible hydrogen electrode.
*j_0 were calculated from Tafel curves using extrapolation method.
†Johnson-Matthey, 20 wt% Pt/XC-72.

MoS_2 (Table 1) and also the j_0 value for most of the reported noble-metal-free HER catalysts (Supplementary Table 1). The high electrode kinetic metrics (including onset potential of -11 mV and the Tafel slope of 36 mV per decade) and large j_0 (only $\sim$1 order of magnitude lower than the value of 7.1×10^{-1} mA cm^{-2} for Pt) highlight the exceptional H_2 evolving efficiency of the new $MoS_2/CoSe_2$ hybrid catalyst.

Material stability. The long-term stability of $MoS_2/CoSe_2$ hybrid catalyst was assayed by means of chronoamperometry measurement ($j \sim t$) with a high catalyst loading of 1 mg cm^{-2} on carbon fibre paper (CFP). This quasi-electrolysis process was performed at a constant potential of -0.7 V vs SCE in 0.5 M H_2SO_4 for 24 h. As shown in Fig. 3c, the current density of $MoS_2/CoSe_2$-modified CFP electrode decreased gradually at the initial 3 h, which then increased quickly over 24 h of continuous operation. We hypothesize that the more efficient HER-active sites in our hybrid materials are the interfaces between MoS_2 and $CoSe_2$, where Co from the support materials could promote the HER kinetics by lowering the Gibbs free energy of adsorbed hydrogen (ΔG_H)[8,29,30]. The severe reducing condition at the initial 3 h caused degradation of external MoS_2 and allowed more electrolyte to access the MoS_2–$CoSe_2$ interfaces (Supplementary Fig. 11; Supplementary Note 1; Supplementary Table 2), yielding the increased HER current density. Remarkably, after 24 h of operation, XPS studies revealed no obvious chemical state change of HER-active S (Fig. 4) and the homogeneous elemental distribution was maintained (Supplementary Fig. 12; Supplementary Note 1), suggesting the robustness of the hybrid

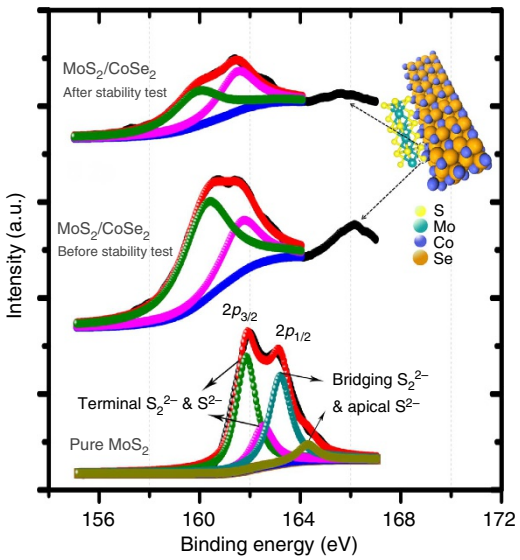

Figure 4 | S 2*p* XPS spectrum analysis. S 2*p* XPS spectra for pure MoS_2, $MoS_2/CoSe_2$ hybrid and $MoS_2/CoSe_2$ hybrid after stability test. The top right corner demonstrates the structure model of $MoS_2/CoSe_2$ hybrid.

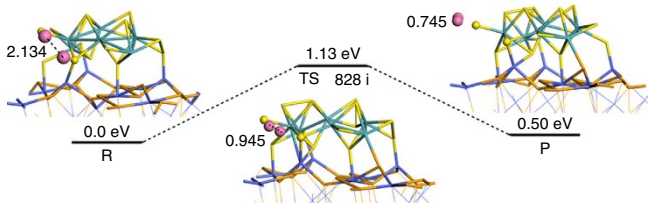

Figure 5 | HER mechanism. Reaction pathway of HER on $MoS_2/CoSe_2$ hybrid according to the Volmer–Tafel route. The calculated distance of two hydrogen atoms and energies are displayed in Å and eV. Blue, orange, azure, yellow and pink indicate Co, Se, Mo, S and H atoms, respectively.

catalyst. By comparison, under the exact same condition, the pure MoS_2 catalyst exhibited a slow but continuous decrease in HER activity. Furthermore, digital photo (inset in Fig. 3c) taken from $MoS_2/CoSe_2$-modified CFP electrode showed vigorous effervescence at 20 h (also Supplementary Movie 1), comparing favourably with the H_2 bubbles formed on free MoS_2-modified electrode. The exceptional long-term durability of our $MoS_2/CoSe_2$ hybrid catalyst suggests the promise for implementing this new catalyst into realistic hydrogen evolution electrode.

HER-enhanced mechanism. The experimentally observed high HER intrinsic activity ($j_0 = 7.3 \times 10^{-2}$ mA cm^{-2}) of $MoS_2/CoSe_2$ hybrid catalyst prompted us to probe the enhanced mechanism. Generally, the value of ΔG_H is considered as a reasonable descriptor of HER activity for a wide variety of catalysts[3,30,31]. An optimum HER activity is suggested to be achieved at value of $\Delta G_H \approx 0$ (ref. 30). Lower ΔG_H will lead to very high surface coverage of H_{ads}, while higher ΔG_H will make the protons bonded too weakly on the catalyst surface, which both lead to the slow HER kinetics[3,30,31]. Previous density functional theory (DFT) calculations[5] showed that MoS_2 edge sites with unsaturated sulfur atoms can lower the ΔG_H approaching to 0 and thus are active for HER, which was later proved by Jaramillo *et al.*[6] experimentally. Recently, Hu and co-workers[13,14] found that amorphous MoS_2 films are particularly HER active and the increased coordinately and structurally unsaturated sulfur atoms led to the enhancement. Furthermore, first-row transition metal ions, especially Co, can promote the HER activity of MoS_2 by coupling with S-edges to lower their ΔG_H from 0.18 to 0.10 eV to afford a faster proton adsorption kinetics[8,29,30]. As to $MoS_2/CoSe_2$ hybrid catalyst, the quasi-amorphous MoS_2 around the $CoSe_2$ may bring in more active edge sites. Meanwhile, the $CoSe_2$ chemically interacts with MoS_2 by forming S–Co bond (Fig. 4 and inset), similar to the XPS peak observed in Co-promoted MoS_3 film[32], which can further improve the HER activity of MoS_2. By contrast, no such XPS peak was found in Fig. 4 for pure MoS_2 catalyst. XPS analyses of the S 2*p* region also exhibit a dramatically decreased electron-binding energy (by $\sim$1.3 eV) after growing MoS_2 on the $CoSe_2$, suggesting the formation of more terminal S_2^{2-} and S^{2-} ions, which are HER active (Fig. 4)[14,19]. Therefore, the $CoSe_2$ nanobelts, a material with decent HER activity by itself, can not only chemically couple with MoS_2 to promote the HER activity, but also serve as an effective support for mediating the growth of MoS_2 to form more terminal S_2^{2-} and S^{2-}. Meanwhile, anchored MoS_2 may also boost the HER-active sites of $CoSe_2$ and these electrocatalytic synergistic effects[33] together lead to the high HER performance of $MoS_2/CoSe_2$ hybrid catalyst.

For the HER in acidic media, two separate pathways (the Volmer–Tafel or the Volmer–Heyrovsky mechanism) have been proposed for reducing H^+ to H_2 (refs 30,34). Specifically, the two distinct mechanisms involve three principal steps, referring to the Volmer (electrochemical hydrogen adsorption: $H_3O^+ + e^- \rightarrow H_{ads} + H_2O$), the Heyrovsky (electrochemical desorption: $H_{ads} + H_3O^+ + e^- \rightarrow H_2\uparrow + H_2O$) and the Tafel (chemical desorption: $H_{ads} + H_{ads} \rightarrow H_2\uparrow$) reactions[30,34]. Tafel slope, an intrinsic property of electrocatalysts, could be used to probe the elementary steps involved in the H_2 evolution. For example, HER kinetic models suggest that Tafel slope of about 120, 40 or 30 mV per decade will be obtained if the Volmer, Heyrovsky or Tafel reaction is the rate-determining step, respectively[34]. The Tafel slope down to $\sim$36 mV per decade for $MoS_2/CoSe_2$ in 0.5 M H_2SO_4 is the lowest value measured till now for MoS_2-based HER catalysts (Supplementary Table 1), even approaching to that of $\sim$30 mV per decade for Pt/C catalysts. This Tafel slope suggests a Tafel-step-determined Volmer–Tafel mechanism works in the $MoS_2/CoSe_2$ catalyst, where the synergistic $CoSe_2$ substrate with decent HER activity presumably contributes to this HER mechanism.

Considering that at least one decade of linearity in Tafel extrapolation at relatively large η is desirable to ensure an accurate Tafel analysis, the calculated Tafel slopes (Fig. 3b) and derived HER mechanism may be inconclusive. To prove the proposed HER mechanism, we performed a computational study on the new $MoS_2/CoSe_2$ catalyst to gain detailed insights into the adsorption, activation and reaction processes (Fig. 5; see Supplementary Methods for computational details). DFT calculations suggested that reactant (**R**) contains two H atoms adsorbed on different sites of the optimized $MoS_2/CoSe_2$ model with H–H distance of 2.134 Å. Two approached H atoms on the side S atoms of MoS_2 cluster then formed a transition state (**TS**) with H–H distance of 0.945 Å and imaginary vibration frequency of 828*i* cm^{-1}. After crossing the **TS**, product (**P**) with a weakly absorbed H_2 molecule (0.745 Å) was formed. The calculated activation barrier of 1.13 eV (30.7 kcal mol^{-1}) for the Tafel-step reaction on $MoS_2/CoSe_2$ hybrid, which can be overcome at a slightly higher η, approaches that of Pt (111) electrode[35], agreeing well with our experimentally observed fast HER kinetics.

Discussion

In conclusion, we demonstrate that an effective and robust hydrogen evolution catalyst can be made by marrying inexpensive transition metal chalcogenides. The new $MoS_2/CoSe_2$ catalyst shows exceptional HER catalytic properties in acidic electrolyte with onset potential of mere -11 mV, a small Tafel slope of 36 mV per decade and a high exchange current density, representing the first non-noble metal catalyst that approaches the performance of state-of-the-art Pt/C catalyst. Inspired by the Nature using transition metals as catalytically active site to construct effective HER catalysts (for example, hydrogenase enzymes)[5,36], we believe that our study here will facilitate the development of newly efficient HER catalysts based on transitional metal chalcogenides.

Methods

Synthesis of $CoSe_2$/DETA nanobelts and $MoS_2/CoSe_2$ hybrid. All chemicals are of analytical grade and were used as received without further purification. First, ultrathin lamellar mesostructured $CoSe_2$/DETA nanobelts were prepared by our recently developed method[20]. Briefly, 0.249 g $Co(OAc)_2 \cdot H_2O$ and 0.173 g Na_2SeO_3 were added into a mixed solution (40 ml) with a volume ratio of $V_{DETA}/V_{DIW} = 2{:}1$ (DIW, deionized water). The obtained wine solution was then transferred into a 50 ml Taflon-lined autoclave, which was sealed and maintained at 180 °C for 16 h. The resulting black floccules were collected by centrifugation (4,000 r.p.m. for 5 min) and washed by absolute ethanol for three times, and the resulting $CoSe_2$/DETA nanobelts were dried for next use. To prepare the $MoS_2/CoSe_2$ hybrid, 10 mg freshly made $CoSe_2$/DETA nanobelts and 10 mg $(NH_4)_2MoS_4$ were dispersed in 10 ml DMF and sonicated for 15 min under ambient conditions. Then, 0.05 ml $N_2H_4 \cdot H_2O$ was added into the suspension. After sonicating for another 15 min to dissolve completely, the mixed solution was transferred into a 50 ml Teflon-lined autoclave, which was sealed and heated in an oven at 200 °C for 10 h and then

cooled to room temperature naturally. The resulting black product was collected by centrifugation (7,000 r.p.m. for 8 min), then washed at least four times by distilled water and absolute ethanol to remove ions and possible remnants, and dried under vacuum at 80 °C for 6 h.

Synthesis of free 3D MoS_2 sheet aggregates. The synthetic procedure of free 3D MoS_2 sheet aggregates is the same with that for preparing $MoS_2/CoSe_2$ hybrid, the only difference is that no $CoSe_2$/DETA nanobelt substrates were added during the synthesis.

Characterization. The samples were characterized by different analytic techniques. X-ray powder diffraction (XRD) was carried out on a Rigaku D/max-rA X-ray diffractometer with Cu Ka radiation ($\lambda = 1.54178$ Å); TEM images, HRTEM images, SAED and an energy-disperse X-ray spectrum (EDS) were taken with a JEOJ-2010 transmission electron microscope with an acceleration voltage of 200 kV. STEM and EDX elemental mapping were performed on JEOL ARM-200F. The X-ray photoelectron spectra (XPS) were recorded on an ESCALab MKII XPS using Mg Ka radiation exciting source. The Fourier transform infrared spectra were measured on a Bruker Vector-22 FT-IR spectrometer at room temperature. Nitrogen sorption was determined by Brunauer, Emmett and Teller measurements with an ASAP-2020 surface area analyzer (see Supplementary Fig. 8 for results). The degradation of external MoS_2 around $CoSe_2$ was determined by the inductively coupled plasma–atomic emission spectrometry analysis using an Atomscan Advantage (Thermo Ash Jarrell Corporation, USA) spectrometer.

Electrocatalytic study. Electrochemical measurements were performed at room temperature using a rotating disk working electrode made of GC (PINE, 5 mm diameter, 0.196 cm^2) connected to a Multipotentiostat (IM6ex, ZAHNER elektrik, Germany). The GC electrode was polished to a mirror finish (No. 40-6365-006, Gamma Micropolish Alumina, Buehler; No.40-7212, Microcloth, Buehler) and thoroughly cleaned before use. Pt wire and SCE were used as counter and reference electrodes, respectively. The potentials reported in our work were vs the RHE through RHE calibration described below.

The preparation method of the working electrodes containing investigated catalysts can be found as follows. In short, 5 mg of catalyst powder was dispersed in 1 ml of 3:1 v/v DIW/isopropanol mixed solvent with 40 µl of Nafion solution (5 wt%, Sigma-Aldrich), then the mixture was ultrasonicated for about 30 min to generate a homogeneous ink. Next, 10 µl of the dispersion was transferred onto the GC disk, leading to the catalyst loading ~ 0.28 mg cm^{-2}. Finally, the as-prepared catalyst film was dried at room temperature. For comparison, bare GC electrode that has been polished and cleaned was also dried for electrochemical measurement.

Before the electrochemical measurement, the electrolyte (0.5 M H_2SO_4) was degassed by bubbling pure hydrogen for at least 30 min to ensure the H_2O/H_2 equilibrium at 0 V vs RHE at a rotation rate of 1,600 r.p.m. The polarization curves were obtained by sweeping the potential from -0.7 to -0.2 V vs SCE at room temperature and 1,600 r.p.m. (to remove the *in situ*-formed H_2 bubbles on the RDE), with a sweep rate of 2 mV s^{-1}. The electrochemical impedance spectroscopy measurement was performed in the same configuration at open circuit potential over a frequency range from 100 kHz to 5 mHz at the amplitude of the sinusoidal voltage of 5 mV and room temperature (see Supplementary Fig. 10 for results). $MoS_2/CoSe_2$ and pure MoS_2-coated CFPs (Toray, 1 cm^2, catalyst loading 1 mg) were used as working electrodes to collect chronoamperometry data at the applied potential of -0.7 V vs SCE. The polarization curves were replotted as overpotential (η) vs log current (log j) to get Tafel plots for assessing the HER kinetics of investigated catalysts. By fitting the linear portion of the Tafel plots to the Tafel equation ($\eta = b \log(j) + a$), the Tafel slope (b) can be obtained. All data were reported without iR compensation.

RHE calibration. In all measurements, we used SCE as the reference electrode. It was calibrated with respect to RHE. The calibration was performed in the high-purity hydrogen-saturated electrolyte with a Pt foil as the working electrode. Cyclic voltammetry was run at a scan rate of 1 mV s^{-1}, and the average of the two potentials at which the current crossed 0 was taken to be the thermodynamic potential for the hydrogen electrode reaction. In 0.5 M H_2SO_4 solution, $E_{RHE} = E_{SCE} + 0.28$ V.

DFT calculations. The computational modelling of the adsorption, activation and reaction processes involved in HER on $MoS_2/CoSe_2$ was performed by periodic DFT with the Vienna *Ab-initio* Simulation Package (VASP). $MoS_2/CoSe_2$ model-building details (Supplementary Figs 13–15), HER mechanism and relevant references are provided in the Supplementary Methods.

References

1. Walter, M. G. *et al.* Solar water splitting cells. *Chem. Rev.* **110,** 6446–6473 (2010).
2. Cook, T. R. *et al.* Solar energy supply and storage for the legacy and nonlegacy worlds. *Chem. Rev.* **110,** 6474–6502 (2010).
3. Greeley, J., Jaramillo, T. F., Bonde, J., Chorkendorff, I. B. & Norskov, J. K. Computational high-throughput screening of electrocatalytic materials for hydrogen evolution. *Nat. Mater.* **5,** 909–913 (2006).
4. Prins, R., Debeer, V. H. J. & Somorjai, G. A. Structure and function of the catalyst and the promoter in Co-Mo hydrodesulfurization catalysts. *Catal. Rev. Sci. Eng.* **31,** 1–41 (1989).
5. Hinnemann, B. *et al.* Biornimetic hydrogen evolution: MoS_2 nanoparticles as catalyst for hydrogen evolution. *J. Am. Chem. Soc.* **127,** 5308–5309 (2005).
6. Jaramillo, T. F. *et al.* Identification of active edge sites for electrochemical H_2 evolution from MoS_2 nanocatalysts. *Science* **317,** 100–102 (2007).
7. Karunadasa, H. I. *et al.* A molecular MoS_2 edge site mimic for catalytic hydrogen generation. *Science* **335,** 698–702 (2012).
8. Bonde, J., Moses, P. G., Jaramillo, T. F., Norskov, J. K. & Chorkendorff, I. Hydrogen evolution on nano-particulate transition metal sulfides. *Faraday Discuss.* **140,** 219–231 (2008).
9. Kibsgaard, J., Chen, Z. B., Reinecke, B. N. & Jaramillo, T. F. Engineering the surface structure of MoS_2 to preferentially expose active edge sites for electrocatalysis. *Nat. Mater.* **11,** 963–969 (2012).
10. Lukowski, M. A. *et al.* Enhanced hydrogen evolution catalysis from chemically exfoliated metallic MoS_2 nanosheets. *J. Am. Chem. Soc.* **135,** 10274–10277 (2013).
11. Kong, D. S. *et al.* Synthesis of MoS_2 and $MoSe_2$ films with vertically aligned layers. *Nano Lett.* **13,** 1341–1347 (2013).
12. Xie, J. F. *et al.* Defect-rich MoS_2 ultrathin nanosheets with additional active edge sites for enhanced electrocatalytic hydrogen evolution. *Adv. Mater.* **25,** 5807–5813 (2013).
13. Merki, D., Fierro, S., Vrubel, H. & Hu, X. L. Amorphous molybdenum sulfide films as catalysts for electrochemical hydrogen production in water. *Chem. Sci.* **2,** 1262–1267 (2011).
14. Vrubel, H., Merki, D. & Hu, X. L. Hydrogen evolution catalyzed by MoS_3 and MoS_2 particles. *Energy Environ. Sci.* **5,** 6136–6144 (2012).
15. Benck, J. D., Chen, Z. B., Kuritzky, L. Y., Forman, A. J. & Jaramillo, T. F. Amorphous molybdenum sulfide catalysts for electrochemical hydrogen production: insights into the origin of their catalytic activity. *ACS Catal.* **2,** 1916–1923 (2012).
16. Liao, L. *et al.* MoS_2 formed on mesoporous graphene as a highly active catalyst for hydrogen evolution. *Adv. Funct. Mater.* **23,** 5326–5333 (2013).
17. Li, Y. G. *et al.* MoS_2 nanoparticles grown on graphene: an advanced catalyst for the hydrogen evolution reaction. *J. Am. Chem. Soc.* **133,** 7296–7299 (2011).
18. Chen, Z. B. *et al.* Core-shell MoO_3-MoS_2 nanowires for hydrogen evolution: a functional design for electrocatalytic materials. *Nano Lett.* **11,** 4168–4175 (2011).
19. Wang, T. Y. *et al.* Enhanced electrocatalytic activity for hydrogen evolution reaction from self-assembled monodispersed molybdenum sulfide nanoparticles on an Au electrode. *Energy Environ. Sci.* **6,** 625–633 (2013).
20. Gao, M. R., Yao, W. T., Yao, H. B. & Yu, S. H. Synthesis of unique ultrathin lamellar mesostructured $CoSe_2$-amine (protonated) nanobelts in a binary solution. *J. Am. Chem. Soc.* **131,** 7486–7487 (2009).
21. Gao, M. R., Xu, Y. F., Jiang, J., Zheng, Y. R. & Yu, S. H. Water oxidation electrocatalyzed by an efficient $Mn_3O_4/CoSe_2$ nanocomposite. *J. Am. Chem. Soc.* **134,** 2930–2933 (2012).
22. Gao, M. R. *et al.* A methanol-tolerant Pt/$CoSe_2$ nanobelt cathode catalyst for direct methanol fuel cells. *Angew. Chem. Int. Ed.* **50,** 4905–4908 (2011).
23. Gao, M. R. *et al.* In situ controllable synthesis of magnetite nanocrystals/$CoSe_2$ hybrid nanobelts and their enhanced catalytic performance. *J. Mater. Chem.* **20,** 9355–9361 (2010).
24. Gao, M. R. *et al.* Mixed-solution synthesis of sea urchin-like NiSe nanofiber assemblies as economical Pt-free catalysts for electrochemical H_2 production. *J. Mater. Chem.* **22,** 13662–13668 (2012).
25. Xu, Y. F., Gao, M. R., Zheng, Y. R., Jiang, J. & Yu, S. H. Nickel/nickel(II) oxide nanoparticles anchored onto cobalt(IV) diselenide nanobelts for the electrochemical production of hydrogen. *Angew. Chem. Int. Ed.* **52,** 8546–8550 (2013).
26. Gao, M. R., Jiang, J. & Yu, S. H. Solution-based synthesis and design of late transition metal chalcogenide materials for oxygen reduction reaction (ORR). *Small* **8,** 13–27 (2012).
27. Gao, M. R., Xu, Y. F., Jiang, J. & Yu, S. H. Nanostructured metal chalcogenides: synthesis, modification, and applications in energy conversion and storage devices. *Chem. Soc. Rev.* **42,** 2986–3017 (2013).
28. Kong, D. S., Cha, J. J., Wang, H. T., Lee, H. R. & Cui, Y. First-row transition metal dichalcogenide catalysts for hydrogen evolution reaction. *Energy Environ. Sci.* **6,** 3553–3558 (2013).
29. Merki, D. & Hu, X. L. Recent developments of molybdenum and tungsten sulfides as hydrogen evolution catalysts. *Energy Environ. Sci.* **4,** 3878–3888 (2011).
30. Parasons, R. The rate of electrolytic hydrogen evolution and the heat of adsorption of hydrogen. *Trans. Faraday Soc.* **54,** 1053–1063 (1958).

31. Norskov, J. K. *et al.* Trends in the exchange current for hydrogen evolution. *J. Electrochem. Soc.* **152,** J23–J26 (2005).
32. Merki, D., Vrubel, H., Rovelli, L., Fierro, S. & Hu, X. L. Fe, Co, and Ni ions promote the catalytic activity of amorphous molybdenum sulfide films for hydrogen evolution. *Chem. Sci.* **3,** 2515–2525 (2012).
33. Chen, W. F. *et al.* Hydrogen-evolution catalysts based on non-noble metal nickel-molybdenum nitride nanosheets. *Angew. Chem. Int. Ed.* **51,** 6131–6135 (2012).
34. Conway, B. E. & Tilak, B. V. Interfacial processes involving electrocatalytic evolution and oxidation of H_2, and the role of chemisorbed H. *Electrochim. Acta* **47,** 3571–3594 (2002).
35. Skulason, E. *et al.* Modeling the electrochemical hydrogen oxidation and evolution reactions on the basis of density functional theory calculations. *J. Phys. Chem. C* **114,** 18182–18197 (2010).
36. DuBois, M. R. & DuBois, D. L. The roles of the first and second coordination spheres in the design of molecular catalysts for H_2 production and oxidation. *Chem. Soc. Rev.* **38,** 62–72 (2009).

Acknowledgements

We acknowledge the funding support from the National Basic Research Program of China (Grants 2010CB934700, 2013CB933900, 2014CB931800 and 2013CB834603), the National Natural Science Foundation of China (Grants 21431006, 91022032, 91227103, 21061160492 and J1030412) and the Chinese Academy of Sciences (Grant KJZD-EW-M01-1).

Author contributions

S.-H.Y. and M.-R.G. conceived the idea. M.-R.G., Y.-R.Z. and Y.-F.X. planned and performed the experiments, collected and analysed the data. J.-X.L. and J.L. performed the DFT calculations. J.J. and Q.G. assisted with the experiments and characterizations. M.-R.G. and S.-H.Y. co-wrote the manuscript. All authors discussed the results and commented on the manuscript.

Additional information

Supplementary Information accompanies this paper at http://www.nature.com/naturecommunications

Competing financial interests: The authors declare no competing financial interests.

Reprints and permission information is available online at http://npg.nature.com/reprintsandpermissions/

How to cite this article: Gao, M.-R. *et al.* An efficient molybdenum disulfide/cobalt diselenide hybrid catalyst for electrochemical hydrogen generation. *Nat. Commun.* 6:5982 doi: 10.1038/ncomms6982 (2015).